JACS
JOURNAL OF THE AMERICAN CHEMICAL SOCIETY

Article

pubs.acs.org/JACS

Structural Zn(II) Implies a Switch from Fully Cooperative to Partly Downhill Folding in Highly Homologous Proteins

Maddalena Palmieri,[†] Gaetano Malgieri,[†] Luigi Russo,[†] Ilaria Baglivo,[†] Sabrina Esposito,[†] Fortuna Netti,[†] Annarita Del Gatto,[‡] Ivan de Paola,[‡] Laura Zaccaro,[‡] Paolo V. Pedone,[†] Carla Isernia,[†] Danilo Milardi,[§] and Roberto Fattorusso*[,†]

[†]Department of Environmental, Biological and Pharmaceutical Science and Technology, Second University of Naples, Via Vivaldi 43, 81100 Caserta, Italy

[‡]Institute of Biostructures and Bioimaging-CNR (Naples), Via Mezzocannone 16, 80134 Naples, Italy

[§]Institute of Biostructures and Bioimaging-CNR (Catania), Viale A. Doria 6, 95125 Catania, Italy

Supporting Information

ABSTRACT: In the funneled landscape, proteins fold to their native states through a stochastic process in which the free energy decreases spontaneously and unfolded, transition, native, and possible intermediate states correspond to local minima or saddle points. Atomic description of the folding pathway appears therefore to be essential for a deep comprehension of the folding mechanism. In metallo-proteins, characterization of the folding pathways becomes even more complex, and therefore, despite their fundamental role in critical biological processes, little is known about their folding and assembly. The study of the mechanisms through which a cofactor influences the protein folding/unfolding reaction has been the rationale of the present study aimed at contributing to the search for cofactors' general roles in protein folding reactions. In particular, we have investigated the folding pathway of two homologous proteins, Ros87, which contains a prokaryotic zinc finger domain, and $Ml4_{52-151}$, lacking the zinc ion. Using a combination of CD, DSC and NMR techniques, we determined the thermodynamics and the structural features, at an atomic level, of the thermal unfolding of Ros87 and compared them to the behavior of $Ml4_{52-151}$. Our results, also corroborated by NMR $^{1}H/^{2}H$ exchange measurements, show that the presence of the structural Zn(II) in Ros87 implies a switch from the $Ml4_{52-151}$ fully cooperative to a two-step unfolding process in which the intermediate converts to the native state through a downhill barrierless transition. This observation, which has never been reported for any metal ion so far, may have a significant role in the understanding of the protein misfolding associated with the presence of metal ions, as observed in neurodegenerative diseases.

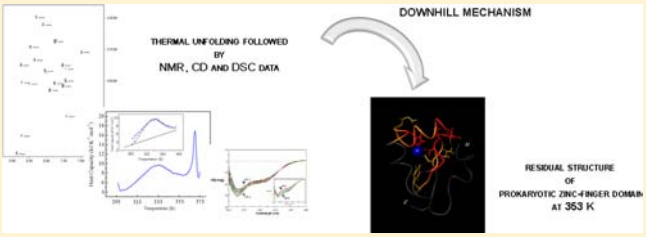

INTRODUCTION

In the conventional paradigm, two-state processes are used to describe the folding of single-domain proteins.[1] The protein molecule is assumed to interconvert between either of two states, folded (or active) and unfolded (or inactive), by crossing a high free-energy barrier. However, because of their thousands of freedom degrees, proteins can in principle exist in many different conformations or microstates. Such inherent complexity is best described by the energy landscape approach,[2] which uses low-dimensional free-energy surfaces obtained by projecting the solvent averaged energy as a function of atomic coordinates onto a few order parameters.[3] In this funneled landscape, proteins fold to their native states through a stochastic process in which the free energy decreases spontaneously and unfolded, transition, native, and possible intermediate states correspond to local minima or a saddle points.[4−7] Atomic description of the folding pathway appears therefore to be essential for a deep comprehension of the folding mechanism. In metallo-proteins, characterization of the folding pathways becomes even more complex. As a matter of fact, metal ions can play an important role not only as local structural stabilizing elements in the native state but also as potential key nucleation points during folding.[8,9] The interplay of the metal cofactors with protein folding and their contribution to the structural stability remains still poorly understood. In some cases, protein folding is totally metal-dependent and involves the coordination of one or more metal ions to drive the folding into the fully functional native conformation, while in other cases metal ions are also capable of binding proteins in a later stage of the folding reaction.[10]

Protein folding mechanisms can be properly characterized using a number of advanced experimental spectroscopic and calorimetric techniques.[4,11,12] In particular, differential scanning calorimetry (DSC)[13−15] combined with nuclear magnetic resonance (NMR) can establish the existence and the height of folding energy barriers and provide site-specific information at atomic resolution on temperature-dependent changes in the

Received: January 30, 2013
Published: March 13, 2013

   dx.doi.org/10.1021/ja4009562 | J. Am. Chem. Soc. 2013, 135, 5220−5228

structure of exchanging states. Furthermore, NMR thermal melts can give an "atom-by-atom" description of the folding process.[3,4]

We have recently characterized the prokaryotic Cys_2His_2 zinc-finger motif, included in the DNA binding region (Ros87) of Ros protein from *A. tumefaciens*, demonstrating that, although possessing a similar zinc coordination sphere, this domain is very different from its eukaryotic counterpart. In particular, the prokaryotic Cys_2His_2 zinc-finger domain adopts a globular fold, consisting of 58 amino acids, arranged in a $\beta\beta\beta\alpha\alpha$ topology and stabilized by an extended hydrophobic core.[16] A large number of Ros homologues has been found in different bacteria having high sequence identity with Ros protein. This high identity surprisingly does not include the zinc coordination sphere: Ros homologues can either change the coordination sphere or lose the metal while still preserving the DNA binding activity.[17]

During the last few years, a considerable amount of research has been aimed at elucidating the folding pathways of proteins with similar structures but diverse sequences, because they provide a critical test of the relationship between native topology and folding pathways.[18−20] In this study, using a combination of CD, DSC and NMR techniques, we determined the thermodynamics and the structural features, at an atomic level, of the thermal unfolding of Ros87 and compared them to the behavior of the DNA binding domain of Ml4 ($Ml4_{52-151}$), one of its zinc lacking homologues. Our results, also corroborated by NMR $^1H/^2H$ exchange measurements, show that the presence of the structural Zn(II) in Ros87 implies a switch from the $Ml4_{52-151}$ fully cooperative to a two-step unfolding process in which the intermediate converts to the native state through a downhill barrierless transition.

MATERIALS AND METHODS

Protein Expression and Purification. Unlabeled, single-labeled (^{15}N Ros87 and $Ml4_{52-151}$), and double-labeled (^{15}N and ^{13}C Ros87 and $Ml4_{52-151}$) proteins used for the ITC, DSC and NMR experiments were overexpressed and purified as previously published.[21]

UV−Vis Spectroscopy. UV−vis spectra were recorded on a Nanodrop2000c spectrophotometer from 200 to 800 nm at 295 K. The apoRos87 concentration was calculated by absorbance at 280 nm.

Co-apoRos87 binding constant was determined in 20 mM phosphate buffer and 4 mM TCEP at pH 6.8 by direct titration of protein solution (81.0 μM) with $CoCl_2$ solution (5.0 mM) up to 3.0 Co/apoRos87 ratio. The absorbance at 340 nm indicative of the $S^- \rightarrow$ Co(II) ligand-to-metal charge-transfer (LCMT) transition[22] was monitored and used to calculate the cobalt binding affinity constant.[23] To estimate the apoRos87 zinc binding constant, the reverse titration experiment was carried out adding $ZnCl_2$ solution (1.0 mM) to Co-apoRos87 complex up to a Zn/apoRos87 ratio of 1.5, and the collected data were fitted as previously reported.[23]

Isothermal Titration Calorimetry (ITC). ITC studies performed on a MicroCal iTC200 calorimeter were used to quantify the binding constant and thermodynamics values of Zn(II) (411 μM) to apoRos87 (17.0 μM) in 20 mM phosphate buffer and 4 mM TCEP at 295 K.

Control experiments to determine the heats of titrant dilution were carried out by making identical injections in the absence of apoRos87 or Zn(II). The net reaction heat was obtained by subtracting the heats of dilution from the corresponding total heat of reaction. The titration data were deconvoluted on the basis of a binding model containing one binding site by a nonlinear least-squares algorithm and the MicroCal Origin 7.0 software.

To estimate accurate enthalpy value $\Delta H_{\text{M-protein}}$ (ΔH), the contributions of the metal buffer enthalpy ($\Delta H_{\text{M-buffer}}$) and buffer protonation enthalpy ($\Delta H_{H^+\text{-buffer}}$)[24,25] to the experimental binding enthalpy (ΔH_{ITC}) were considered, assuming that the number of protons released over the course of the reaction is 2.0. $\Delta H_{\text{M-buffer}}$ and $\Delta H_{H^+\text{-buffer}}$ calculated values are negligible.

Differential Scanning Calorimetry (DSC). DSC experiments were carried out with a MicroCal VP-DSC calorimeter. Protein solutions were prepared after extensive dialysis against the buffer. All protein samples, after a degassing process, were heated at 1 K/min in the temperature range 293−373 K. An extra external pressure of about 29 psi was applied to the solution to prevent the formation of air bubbles during heating. In all measurements, the buffer from the last dialysis step was used in the reference cell of the calorimeter. To ensure a proper equilibration of the calorimeter, several buffer−buffer heating scans were routinely performed prior to the measurement. Only after obtaining invariant buffer−buffer baselines were protein scans performed. Additional buffer−buffer baselines were obtained immediately after the protein scans to rule out uncontrolled drifts in instrumental baseline. For each protein, three independent DSC experiments were carried out under the same buffer conditions but with different protein concentrations within the 60−250 μM range. To obtain the heat capacity Cp curves, buffer−buffer baselines were recorded at the same scanning rate and then subtracted from sample curves, as previously described.[26−28] In most experiments, one or several heating−cooling cycles were carried out to determine the reversibility of the denaturation process. To obtain the excess heat capacity profiles (Cp_{exc}) of $Ml4_{52-151}$, DSC curves, after instrumental baseline correction, were subtracted from a baseline obtained by a third-order polynomial fit of the pre- (Cp^N) and post- (Cp^U) transition Cp trends, as shown in Figure 2 and elsewhere recommended.[29] Experimental values of the absolute heat capacity of Ros87 were calculated at different protein concentrations from the experimental thermograms using the software provided by MicroCal as previously described.[11] The partial specific volume of Ros87 was calculated according to the equation proposed by Fischer.[30] For Ros87, the native baseline could not be easily extrapolated from the DSC thermogram, as we have done for $Ml4_{52-151}$. Alternatively to an extrapolation from experimental curves, we have employed a previously proposed empirical equation in which the heat capacity versus T function is directly calculated from the molecular mass of the protein.

NMR Spectroscopy. NMR samples contained 1 mM ^{15}N Ros87, $Ml4_{52-151}$ or $^{15}N-^{13}C$ Ros87, $Ml4_{52-151}$, 20 mM phosphate buffer, 0.2 M NaCl, and only in the case of Ros87, also 4 mM TCEP, adjusted at pH 6.8, and 90% H_2O/10% ^2H_2O or 100% ^2H_2O only for the $^1H/^2H$ exchange experiments. All of the NMR experiments were acquired on a Varian Unity INOVA 500 MHz spectrometer. For the thermal unfolding experiments, a series of $^1H-^{15}N$ and $^1H-^{13}C$ HSQC spectra were acquired increasing temperatures at regular intervals of 5 K from 278 to 353 K with the following parameters: the number of complex points was 256 for ^{15}N (F1), 2048 for ^1H (F2), 512 for ^{13}C (F1), and 2048 ^1H (F2). Each chemical shift versus temperature data set acquired was then fitted using a nonlinear least-squares method to obtain all atomic sigmoidal unfolding curves reported and the related T_m.[4] All of the unfolding curves were obtained using the program GraphPad Prism5. $^1H^N$ and ^{15}N chemical shift perturbations at 353 K were estimated by using the following equation[31] and reported onto Ros87 structure:

$$\Delta\delta = [(\Delta H^2 + (\Delta N/5)^2)/2]^{1/2}$$

where ΔH and ΔN are the differences between the chemical shifts at 298 and 353 K, respectively.

To perform H/D exchange measurements, ^{15}N Ros87 and $Ml4_{52-151}$ proteins were dissolved in D_2O, and a series of a FAST-$^1H-^{15}N$-HSQC[32] at 298 K were collected utilizing the number of complex points 256 for ^{15}N (F1) and 2048 for ^1H (F2), at regular intervals. The first experiments were started 8 and 13 min after initial suspension of the Ros87 and $Ml4_{52-151}$ proteins, respectively. The experiments were acquired on Ros87 at p^2H 6.7, and for $Ml4_{52-151}$ the p^2H value was 6.89. Experiments were successively also performed at p^2H 7.1 and p^2H 7.3 for the two proteins respectively to ascertain the mechanism of exchange. The decays of volume integrals of the cross-

dx.doi.org/10.1021/ja4009562 | J. Am. Chem. Soc. 2013, 135, 5220−5228

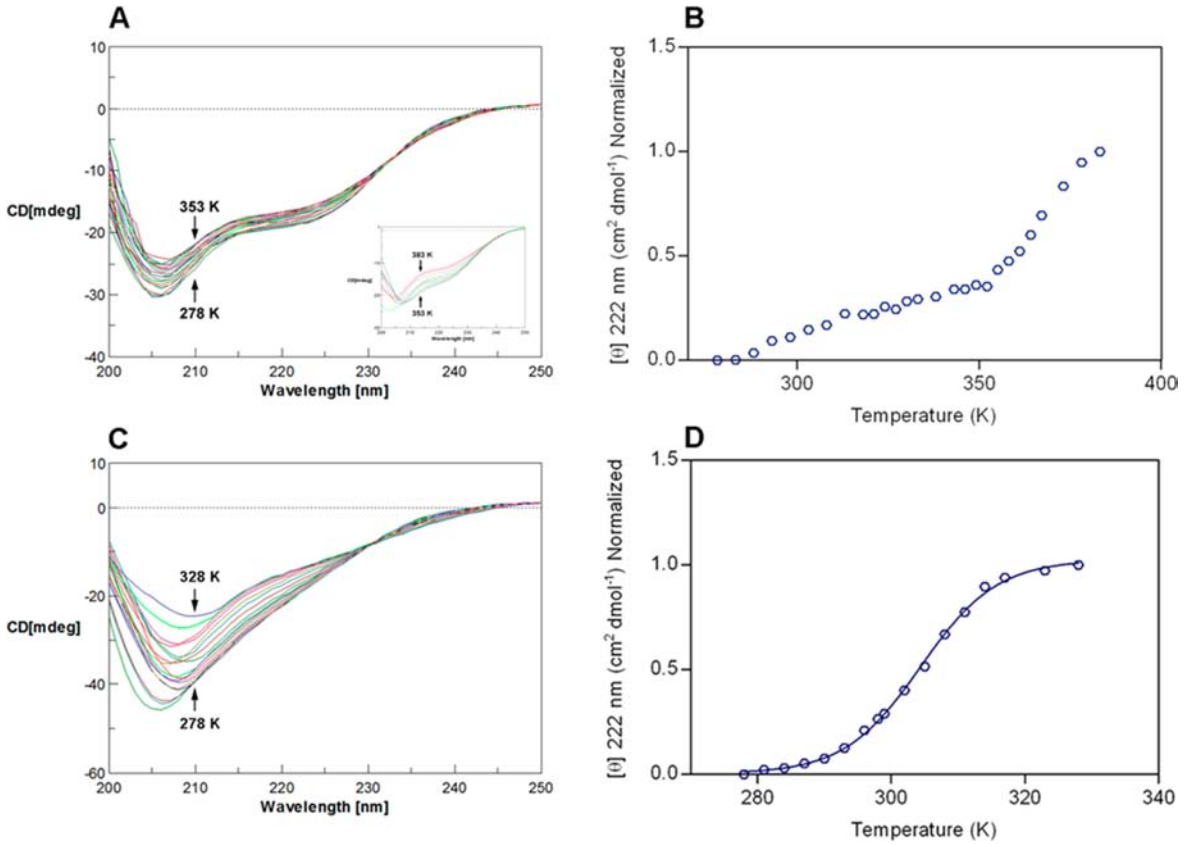

Figure 1. Thermal unfolding of Ros87 and $Ml4_{52-151}$ followed by circular dichroism. (A) Thermal unfolding of Ros87 carried out in the range of 278−383 K at regular intervals of 4 K: the figure shows the isodichroic point at 233 nm observable in the range of 278−353 K, and the inset reports the spectra recorded in the range of 353−383 K. (B) Melting curve of Ros87 monitored by CD at 222 nm. (C) Thermal unfolding of $Ml4_{52-151}$ carried out in the range of 278−328 K at regular intervals of 3 K. (D) Melting curve of $Ml4_{52-151}$ monitored by CD at 222 nm. The blue line is a fit to a two-state model.

peaks were fitted to a single exponential function ($I_{(t)} = I_0$*exp($-k_{ex}$) + A), using the program KaleidaGraph (AbelbeckSoftware), to obtain k_{ex} that is experimental exchange rate. Exchange rates were expressed as protection factors (PF), equal to the ratio k_{int}/k_{ex}, where k_{ex} is the observed rate constant and k_{int} is the exchange rate constant for an $^1H^N$, at the same p^2H, in a small peptide of equivalent sequence computed from empirical, nearest neighbor rules.[33] The intrinsic rates of exchange from the denatured state (k_{int}) were calculated using the SPHERE server.[34] The hydrogen exchange process can be considered as a two-state process, in which EX2 mechanism is defined as reported.[35−38] NMR experiments were processed by using Varian (VNMR6.1B) software. ^1H, ^{13}C, and ^{15}N chemical shifts were calibrated indirectly by using external references. The program XEASY[39] was used to analyze and assign the spectra. The structures were visualized by using the program MOLMOL.[40]

CD Spectroscopy. Protein samples were prepared in 10 mL of 20 mM phosphate buffer containing 0.2 M NaCl adjusted at pH 6.8 and only in the case of Ros87 with 4 mM TCEP. The thermal denaturation of the Ros87 and $Ml4_{52-151}$ proteins was evaluated using a JASCOJ-815 CD spectropolarimeter equipped with Peltier temperature control. CD spectra were measured at 4 K intervals in the 278−383 K range for Ros87 and from 278 to 328 K at regular intervals of 3 K for $Ml4_{52-151}$. After the final measurement at 373 K, the samples were cooled to 298 K, and a final set of spectra was collected. The experiments were conducted on 28 and 21 μM of Ros87 and $Ml4_{52-151}$ proteins, respectively, and data were collected using a quartz cuvette with a 1 cm pathlength in the 200−260 nm wavelength range with a data pitch of 1 nm. All data were recorded with a bandwidth of 1 nm with a scanning speed of 50 nm/min and normalized against reference spectra to remove the background contribution of buffer. The data obtained were fitted into two-state folding model.[41]

RESULTS

Unstructured apoRos87 Binds Zn(II) with High Affinity. Ros87 structural features in the absence of zinc ion at neutral pH have been investigated by $^1H-^{15}N$ HSQC analysis to have a better description of the prokaryotic zinc finger−Zn(II) interaction: the data obtained indicate that apoRos87 is mostly unstructured (Figure S1). Successively, to estimate the zinc binding constant, a procedure based on the competition of cobalt and zinc ions has been used as an indirect spectroscopic method for monitoring the zinc binding to the apoRos87. Co- and Zn-apoRos87 binding constants have then been determined by means of UV−vis spectrophotometry[23,42] and turned out to be 8.3 (±2) × 10^{-6} M and 3.6 (±0.8) × 10^{-8} M, respectively (Figure S2). Furthermore, the thermodynamic parameters of Zn-apoRos87 binding has been also evaluated by isothermal titration calorimetry (ITC)[43,44] at 295 K. K_d, ΔH, and ΔS obtained values are 2.0 (±0.9) × 10^{-8} M, −23.8 kcal/mol (±0.3), and −45.4 cal/mol/deg (±0.6), respectively (Figure S3).

$Ml4_{52-151}$ and Ros87 Share a Similar Fold. The complete ^1H, ^{15}N, and ^{13}C NMR chemical shift assignment of the $Ml4_{52-151}$ DNA binding domain[45] has been processed by the CS23D server[46] to obtain a $Ml4_{52-151}$ model structure (Figure S4). $Ml4_{52-151}$ tertiary fold is nearly identical to that of the zinc containing Ros87 (Figure S5). This is expected on the basis of their high sequence identity (more than 60% within the folded region, with the 15 residues constituting the hydrophobic core

dx.doi.org/10.1021/ja4009562 | J. Am. Chem. Soc. 2013, 135, 5220−5228

wholly conserved), the similar chemical shifts of the conserved residues, and their capability to bind the same DNA target sequence with high affinity.[17]

Thermal Unfolding of Ml4$_{52-151}$ and Ros87. Initially, thermal unfolding of Ros87 and Ml4$_{52-151}$ has been investigated by CD spectroscopy (Figure 1A,C). The two proteins show diverse curve shapes suggesting different unfolding behaviors. In particular, the reversible thermal unfolding profile of Ml4$_{52-151}$ encompasses the temperature range between 290 and 320 K and can be fitted to a classical two-state model with melting temperature of 306 K[41] (Figure 1D). Differently, the unfolding pathway of Ros87 is considerably more complicated, spanning a temperature range of 83 K, between 295 and 378 K, and cannot be described using a simple two-state model (Figure 1B). Interestingly, while Ml4$_{52-151}$ CD unfolding curves present a clear isodichroic point at 231 nm, indicative of a reversible transition, for Ros87 unfolding an isodichroic point, at 233 nm, is observable only for CD spectra recorded in the 278−353 K range[11] (Figure 1A,C).

According to these results, the DSC thermograms of the two proteins are profoundly different (Figures 2 and 3).

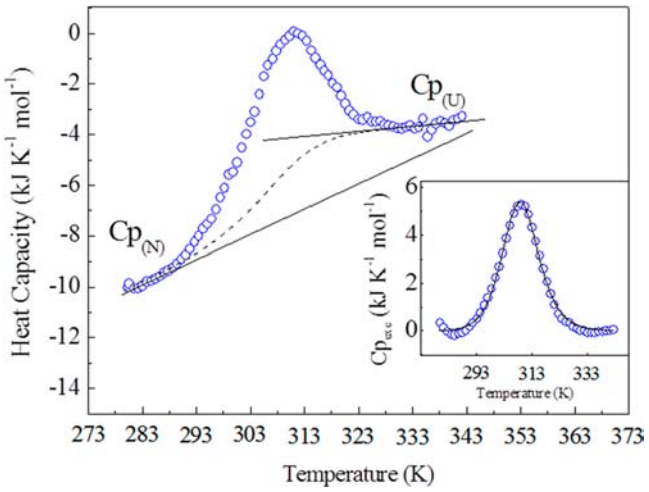

Figure 2. Representative profile of thermally induced unfolding of Ml4$_{52-151}$ monitored by DSC (solid line) and its baseline (dotted line). The inset shows excess heat capacity (Cp_{exc}) of Ml4$_{52-151}$ obtained after baseline subtraction from the DSC thermogram.

In particular, DSC analysis showed that the thermally induced unfolding of Ml4$_{52-151}$ is reversible and can be described as a two-state cooperative transition because the van't Hoff ratio, $\Delta H_{VH}/\Delta H_{cal}$, where ΔH_{VH} is the fitting derived unfolding enthalpy and ΔH_{cal} is the measured calorimetric unfolding enthalpy, is r^{VH} = 1.1 (Table 1).

$Cp_{(N)}$ and $Cp_{(U)}$ do not cross within the transition regions, further supporting the cooperative thermal unfolding of Ml4$_{52-151}$ (Figure 2). Moreover, the DSC-derived unfolding parameters are in good agreement with the corresponding values obtained via CD analysis[41] (Table 1). Differently, the thermal transition of Ros87 consists of a first broad, reversible endotherm centered at about 333 K followed by a second irreversible sharp endotherm centered at 365 K (Figure 3) suggesting an unfolding process with two steps separated by a folding intermediate. The native baseline of the first transition could not be directly extrapolated from the DSC thermogram, as done for Ml4$_{52-151}$. As an alternative to direct extrapolation, we used a previously proposed equation,[47] in which the native

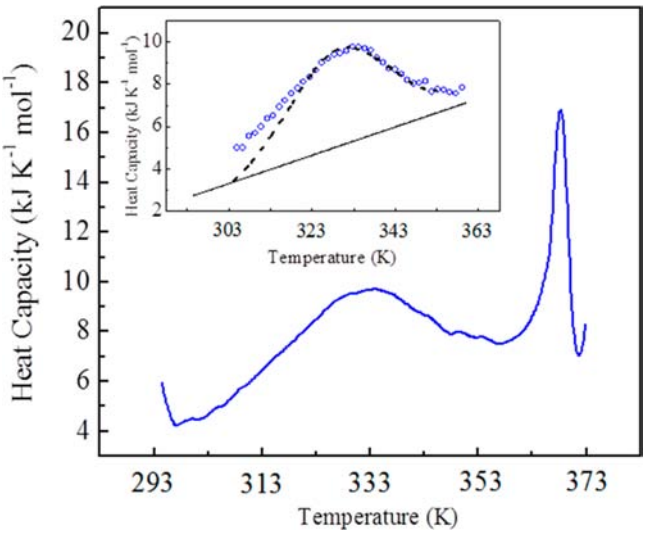

Figure 3. Representative profile of thermally induced unfolding of Ros87 monitored by DSC (blue curve). In the inset the curve traced with dashed lines is the fit to variable-barrier energy model. The native baseline calculated is shown as a continuous line.

Table 1. Thermodynamic Parameters for Ml4$_{52-151}$ Derived from CD and DSC Analysis

thermodynamic parameters for Ml4$_{52-151}$	CD	DSC
T_m (K)	306 ± 1.5	309.23 ± 0.5
ΔH_{VH} (kcal/mol)	37 ± 2.5	32.70 ± 3.1
ΔH_{cal} (kcal/mol)		29.40 ± 3.0
ΔCp (kcal/mol·K)	1 ± 0.3	1.50 ± 0.1

heat capacity versus temperature is directly calculated from the molecular weight of the protein. At first, we fitted the DSC thermogram of Ros87 by the classic two-state formalism (Figure S6). The obtained ΔH_{VH} is significantly different from ΔH_{cal}, further indicating that the two-state model is inadequate to describe Ros87 thermal unfolding. Hence, a more quantitative analysis of the DSC thermogram has been performed by estimating free-energy surface for folding and the height of the barrier separating the native and unfolded conformational ensembles. This has been done by fitting the DSC thermogram to a variable-barrier energy model proposed by Muñoz and Sanchez-Ruiz.[48] The best fit to the DSC thermogram with the variable-barrier model resulted in the following parameters: $\Sigma\alpha$ = 175 kJ mol^{-1}, T_0 = 332.8 K, and β = 2.1 kJ mol^{-1}. The inset of Figure 3 shows a fit with a β-value that results in a marginal free-energy barrier (i.e., $\lesssim 2RT$), suggesting a downhill scenario. Furthermore, Figure 4 shows the probability distribution as a function of H for Ros87 as obtained from the best fit reported in Figure 3.

The shape of the free-energy functional is clearly downhill. The probability distribution changes as expected for a one-state transition. The distribution is unimodal at all temperatures, with the maximum probability shifting from low-enthalpy values at low temperature to high-enthalpy values at high temperature. The second irreversible transition can be linked to the final metal loss, which indeed requires a large ΔH as indicated by ITC thermodynamics data, similar to that already observed in SOD protein unfolding.[49] For consistency with the analysis of the DSC curve of Ros87, we also fitted the calorimetric curve of Ml4$_{52-151}$ with the variable barrier model (Figure S7). The value of β obtained is 5.2 kJ/mol and thus

dx.doi.org/10.1021/ja4009562 | J. Am. Chem. Soc. 2013, 135, 5220−5228

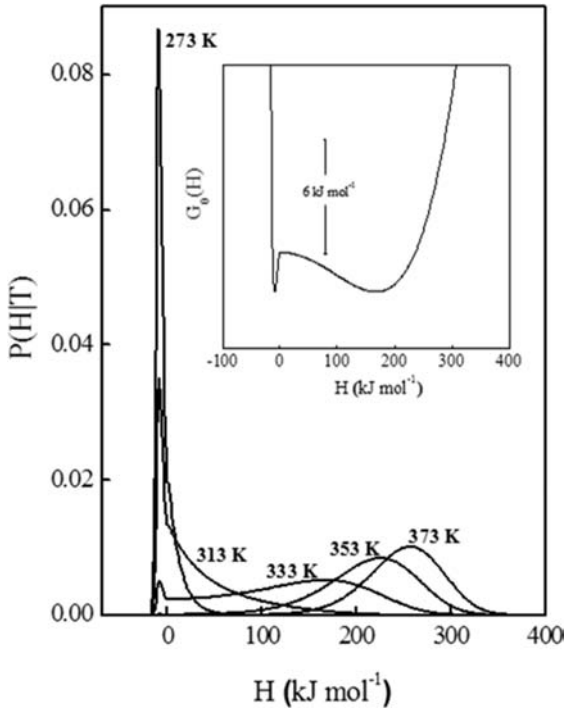

Figure 4. Probability distributions $[P(H|T)]$ of Ros87 at different temperatures calculated with the parameters from the fit described in the text. The inset shows the plot of free-energy $G_0(H)$ versus enthalpy.

confirms the presence of a significant energy barrier for the unfolding of $Ml4_{52-151}$.

In addition, the thermal unfolding of Ros87 and $Ml4_{52-151}$ was examined using NMR spectroscopy. Temperature-induced chemical shift perturbations have been monitored in a series of $^{1}H-^{15}N$ and $^{1}H-^{13}C$ HSQC spectra acquired in a range from 278 to 353 K at regular intervals of 5 K. Interestingly, $Ml4_{52-151}$ signals disappeared at about 308 K and reappeared with typical random coil chemical shift values at 313 K (Figure S8). This behavior is in agreement with a two-state thermal unfolding, consistent with a folding/unfolding conformational exchange in the micro- to millisecond time scale.[50,51] On the contrary, Ros87 ^{1}H, ^{15}N, and ^{13}C resonances exhibited a continuous chemical shift variation in the 278−353 K range, indicating a faster protein folding process in microseconds,[52,53] and some of them still preserved a good spectral dispersion at 353 K (Figure S9). The analysis of the NMR thermal unfolding curves revealed that most of the residues show a single sigmoidal behavior with only a small number of them sharing a more complex behavior (Figure S10). Totally, we obtained 148 curves (68 $N-H^N$, 80 H_α and H_β) with different midpoint temperatures (T_m) distributed in the range between 300 and 350 K, which corresponds to the first transition described by the DSC analysis. Importantly, this broad range of atomic T_m is approximately Gaussian, with a mean value of ~326 K (Figure 5) with a standard deviation of 8 K. The sum of atomic unfolding processes obtained by NMR therefore corresponds to the first global process described by DSC and CD.

Moreover, it is important to note that groups of protons with similar T_m values are not localized in specific structural regions (Figure 6).

Ros87 does not show any clear hierarchical behavior in the transition from the folded state to the intermediate state: the

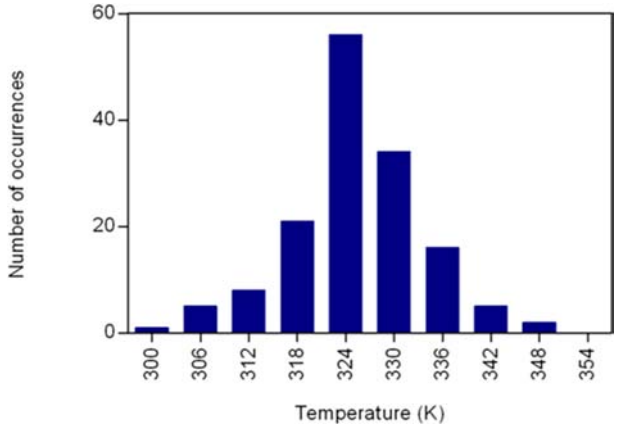

Figure 5. Histogram of T_m values for all 148 protons of Ros87.

continuous unfolding of Ros87 is therefore not characterized by a sequence of local unfolding events. Overall, the NMR analysis confirms that Ros87 thermal unfolding consists of a first noncooperative reversible transition in the 300−350 K range defining a downhill scenario. Interestingly, this unfolding pathway leads to an intermediate with a residual tertiary structure stabilized by the presence of the metal ion. As DSC analysis indicates, a second irreversible transition of Ros87, involving higher *Cp*, occurs between 370 and 390 K and is likely due to final loss of the metal ion and of the residual structure. Importantly, mapping of the ^{15}N and $^{1}H^N$ chemical shift variations occurring in the 298−353 K range onto the Ros87 structure derived at 298 K (Figure 7) allows one to find essential structural details of the Ros87 unfolding intermediate state at 353 K.

In particular, the smallest chemical shift perturbations are observed in the β-hairpin (Cys24-Phe31) containing the two coordinating cysteines, in the last turn of the first helix, comprising the second coordinating histidine, and in the entire second helix (Glu47-Trp53), including the side-chain indolic amide (Figure S9).

Hydrogen/Deuterium Exchange of $Ml4_{52-151}$ and Ros87. $^{1}H/^{2}H$ exchange measurements at equilibrium at 298 K well support the previously shown data; in particular, slowly exchanging amide protons in Ros87 occur following a EX2 mechanism, because no correlation is observed between the k_{ex} measured at different pH values and protection factors range from 6.6 to 8.02 (with an average value of 7.3). Distribution of these values onto protein structure (Figure 8A) shows that most of the Ros87 slowly exchanging protons are localized in hydrogen-bonded secondary structures[54,55] within the residual structure defined by the thermal unfolding. On the contrary, in $Ml4_{52-151}$ the slowly exchanging amide protons occurring with a EX2 regime are well distributed along the entire structure (Figure 8B) and have protection factors ranging from 5.8 to 6.9 (with an average value of 6.2).

■ DISCUSSION

Despite their fundamental role in critical biological processes, little is known about the mechanisms of metallo-protein folding and assembly.[56] Even so, it is clear that cofactors such as metal ions can have significant effects on protein stability, folding, or unfolding pathways; there is an abundance of examples in which engineering a zinc site results in important changes in thermodynamic stability of the metallo-protein.[57] The study of the mechanisms through which a cofactor influences the

dx.doi.org/10.1021/ja4009562 | J. Am. Chem. Soc. 2013, 135, 5220−5228

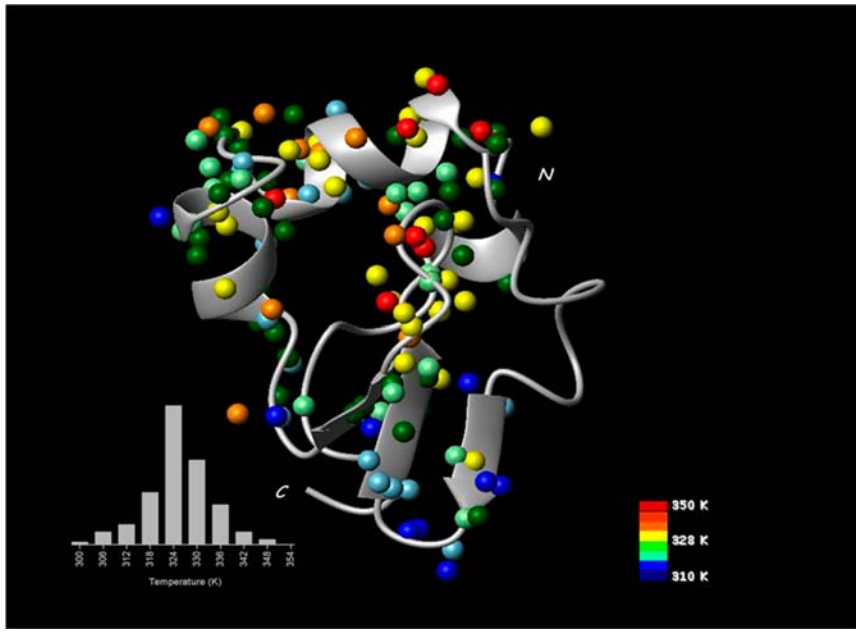

Figure 6. "Atom-by-atom" unfolding behavior of Ros87 in 278−353 K range. Ribbon drawing of Ros87 structure showing the thermal stability of the 148 protons mapped on their corresponding atoms. The inset shows the T_m scale. The color displayed for each atom corresponds to the T_m for sigmoidal transition.

Figure 7. Ros87 residual structure at 353 K. Mapping of native-like chemical shifts onto Ros87 structure highlighting the folding intermediate forming at 353 K. In red is amino acid with $\Delta\delta$ (H^N and N) < 0.3 ppm, and in orange is amino acid with 0.3 < $\Delta\delta$ < 0.5. Side chains involved in zinc coordination and in hydrophobic core formation are displayed.

protein folding/unfolding reaction has been the rationale of the present study aimed at contributing to the search for cofactors general roles in protein folding reactions. Here, we have investigated the effect of the presence/absence of the zinc ion on the folding pathway of Ros87 and $Ml4_{52-151}$, which have similar three-dimensional structures but differ precisely in the residues involved in the zinc coordination site, which tie together the protein core. We first determined the binding affinity and thermodynamic parameters characterizing Zn-apoRos87 complex formation. Interestingly, this reaction appears to be driven by a large enthalpic advantage, which compensates the global entropic costs required for the metal-induced folding of apoRos87 disordered structure. This thermodynamic behavior of complex formation is different from that usually observed in the eukaryotic counterparts: in fact, in eukaryotic zinc fingers, due to the smaller domains a neat entropic advantage comparable to the enthalpic contribution is generally observed.[43,44] $Ml4_{52-151}$ and Ros87 thermal-induced unfolding occurs through different pathways as demonstrated by CD, DSC and NMR analyses. $Ml4_{52-151}$ experiences a two-state cooperative unfolding with rather low melting temperature and ΔH_m (Table 1). The absence of

dx.doi.org/10.1021/ja4009562 | J. Am. Chem. Soc. 2013, 135, 5220−5228

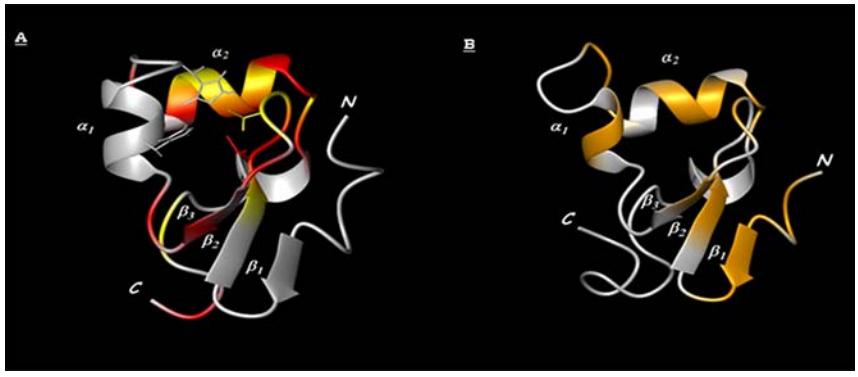

Figure 8. Hydrogen/deuterium exchange of Ros87 and $Ml4_{52-151}$. (A) Ribbon drawing of Ros87 structure showing the location of protection factors with high (>7, in red), medium (between 6 and 7, in yellow), and low (<6, in white) values. (B) Ribbon drawing of $Ml4_{52-151}$ structure showing the location of protection factors with medium (between 6 and 7, in yellow) and low (<6, in white) values.

chemical shift variations and the disappearing of the resonances around the melting temperature during thermal unfolding are in agreement with a two-state unfolding mechanism. The presence of the structural zinc ion in Ros87 affects profoundly its folding pathway. In the earliest stages of Ros87 folding, the recruitment of zinc ion and the consequent intermediate formation are allowed by a major enthalpy advantage,[58] which is comparable to the ΔH_{ITC} required for the native metal binding, and likely compensates the reduction of the solvent−protein system global entropy. The structural details of this folding intermediate can be hypothesized on the basis of the Ros87 resonances still visible at 353 K in the NMR spectra. The residual structure can profitably be evaluated at the light of the folding pathway recently described for the smaller eukaryotic domain.[59] In this computational study, the folding mechanism in classical eukaryotic zinc finger is proposed to begin with the metal coordination by two cysteines: successively the first histidine is recruited inducing the formation of a small hydrophobic core that stabilizes the $\beta\beta\alpha$ motif together with the zinc coordination.[57,60] The second histidine then binds the metal so that the helix folds completing the folding pathway. The collected NMR data describing the thermal unfolding pathway of the prokaryotic zinc finger domain suggest the presence of an intermediate state once the zinc ion is coordinated by three of the four native ligands. At the same time, a proto-hydrophobic core is formed. In detail, the two cysteines appear to stabilize the β-turn when coordinating, probably allowing Glu26 and Trp53 to form a native-like interaction that anchors the second helix to the zinc coordination site (Figure 7). Differently from what was described for the folding pathway of the eukaryotic zinc finger, in the prokaryotic zinc finger the second histidine is the third zinc ligand that contributes to extend the hydrophobic core allowing His41 and Met44 to assume a native-like conformation. Very likely, the forth zinc coordinating position is not occupied by the native first histidine, which is included in the region of the first helix that is not structured in the folding intermediate (Figure 7).

The disappearance of the remainder of the (non metal-binding) peaks in the high temperature Ros87 spectrum suggests that the regions of the protein outside the metal-binding site are not highly unfolded, and are rather involved in conformational exchange processes likely reflecting a somewhat compact ensemble, consistent with considerable remaining secondary structure as shown by CD at this temperature.

Amide protection factors obtained from solvent exchange rates support significant differences in the folding properties of the two proteins. While it is clear that slow exchanging protons in the native state at 298 K do not necessarily reflect regions of stability in the intermediate state, in an on pathway three-state system (U ↔ I ↔ N), the existence of folding intermediate has a profound effect on the hydrogen/deuterium exchange behavior.[61,62] Slowly exchanging amides of Ros87, which are entirely included within the residual intermediate structure identified at high temperature, outline the presence of a similar intermediate within Ros87 folding pathway at room temperature. On the other hand, $Ml4_{52-151}$ amides, having lower protection factor (see above), are homogenously distributed in all of the secondary structure elements of the protein, indicating that likely a single unfolding event breaks most parts of the hydrogen-bond network and causes the overall unfolding. This behavior is in agreement with the cooperative thermal unfolding pathway identified for $Ml4_{52-151}$ protein.[63]

Downhill folding has been characterized as a unique thermodynamic state consisting of an ensemble of conformations that loses structure gradually as protein stability decreases.[2] Muñoz and co-workers have identified and described the downhill folding pathway of the BBL domain,[4,11,48,64] using a number of techniques, including DSC and high-resolution NMR approaches. Another example of a downhill scenario has been identified in the folding of GpW.[65] We have used CD, DSC and NMR to verify that in prokaryotic zinc finger domains the transition of the intermediate state to the native state occurs via downhill folding. DSC thermodynamic parameters indicate that the free energy of the intermediate is comparable to that of the native state, suggesting that the transition from the intermediate to the native state can occur via downhill folding: the fitting of the DSC thermogram to a variable-barrier energy model[48]provided a value of β = 2.1 kJ mol^{-1}, typical of a downhill folding. The NMR analysis corroborated this scenario; as for BBL protein, all of the proton resonances reported as a function of the temperature show sigmoidal curves. No hierarchical behavior is observed in the localization of the unfolding temperatures of the single atoms (Figure 6), and their distribution has a Gaussian shape (Figure 5). Finally, an isodichroic point at 231 nm is present in the CD spectra in the 275−353 K range, congruently with a reversible downhill folding,[11] while it is not visible during the irreversible transition occurring between 356 and 383 K (Figure 1A).

dx.doi.org/10.1021/ja4009562 | J. Am. Chem. Soc. 2013, 135, 5220−5228

These considerations indicate that the rate-limiting step in this folding process is represented by the zinc coordination, which induces the formation of a partially folded intermediate. Once the folding intermediate forms, the protein reaches its native state with a noncooperative downhill mechanism. Interestingly, in the homologous $Ml4_{52-151}$, the structural zinc is dispensable, thus implying a totally different pathway and a strongly reduced thermodynamic stability.

CONCLUSIONS

Indeed, our data point out that the metal ion coordination stabilizes a folding intermediate having a small energetic difference from the native state, therefore inducing a partly downhill folding mechanism. Fully downhill folding proteins have been predicted to be rather rare in nature, because they miss a large folding barrier that can guard against aggregation and proteolysis in keeping unfolded structures less populated.[66] Conversely, partly downhill folding pathways driven by the metal coordination and characterized by variable energy folding barriers could be diffused among metallo-proteins. Additionally, one can infer that a native protein folding pathway could be modified in the presence of metal ions, switching it to a more delicate downhill mechanism. This would enhance the possibility of misfolding events, also through the stabilization of intermediate states that have been proven to be relevant in many pathological processes, such as the formation of the amyloid fibers responsible for several neurodegenerative diseases.

ASSOCIATED CONTENT

Supporting Information

NMR spectra of apoRos87, $Ml4_{52-151}$, and Ros87 at 313 and 353 K, respectively. Representative melting curves of Ros87 protons. Superposition of Ros87 and $Ml4_{52-151}$ structures. UV−vis reverse titrations spectra and curves of apoRos87 and Co-apoRos87. Binding isotherm of Zn(II) binding to apoRos87. Evaluation of Ros87 DSC thermogram by two-state formalism and $Ml4_{52-151}$ thermogram by variable barrier model. This material is available free of charge via the Internet at http://pubs.acs.org.

AUTHOR INFORMATION

Corresponding Author

roberto.fattorusso@unina2.it

Notes

The authors declare no competing financial interest.

ACKNOWLEDGMENTS

We thank Dr. Vincenzo Piscopo, Mr. Maurizio Muselli, and Mr. Marco Mammucari for excellent technical assistance. This work was partially funded by grants PRIN 2010 2010M2JARJ_002 and Programma MERIT RBNE08HWLZ_014 from Ministero dell' Istruzione, dell'Università e della Ricerca (MIUR).

REFERENCES

(1) Tanford, C. *Adv. Protein Chem.* **1968**, *23*, 121.
(2) Bryngelson, J. D.; Onuchic, J. N.; Socci, N. D.; Wolynes, P. G. *Proteins* **1995**, *21*, 167.
(3) Halskau, O.; Perez-Jimenez, R.; Ibarra-Molero, B.; Underhaug, J.; Muñoz, V.; Martinez, A.; Sanchez-Ruiz, J. M. *Proc. Natl. Acad. Sci. U.S.A.* **2008**, *105*, 8625.
(4) Sadqi, M.; Fushman, D.; Muñoz, V. *Nature* **2006**, *442*, 317.
(5) Brockwell, D. J.; Radford, S. E. *Curr. Opin. Struct. Biol.* **2007**, *17*, 30.
(6) Korzhnev, D. M.; Salvatella, X.; Vendruscolo, M.; Di Nardo, A. A.; Davidson, A. R.; Dobson, C. M.; Kay, L. E. *Nature* **2004**, *430*, 586.
(7) Chen, Y.; Ding, F.; Nie, H.; Serohijos, A. W.; Sharma, S.; Wilcox, K. C.; Yin, S.; Dokholyan, N. V. *Arch. Biochem. Biophys.* **2008**, *469*, 4.
(8) Coyne, H. J.; Ciofi-Baffoni, S.; Banci, L.; Bertini, I.; Zhang, L.; George, G. N.; Winge, D. R. *J. Biol. Chem.* **2007**, *282*, 8926.
(9) Ikeguchi, M.; Kuwajima, K.; Sugai, S. *J. Biochem.* **1986**, *99*, 1191.
(10) Wittung-Stafshede, P. *Acc. Chem. Res.* **2002**, *35*, 201.
(11) Garcia-Mira, M. M.; Sadqi, M.; Fischer, N.; Sanchez-Ruiz, J. M.; Muñoz, V. *Science* **2002**, *298*, 2191.
(12) Muñoz, V. *Int. J. Quantum Chem.* **2002**, *90*, 1522.
(13) Sanchez-Ruiz, J. M. *Annu. Rev. Phys. Chem.* **2011**, *62*, 231.
(14) Robertson, A. D.; Murphy, K. P. *Chem. Rev.* **1997**, *97*, 1251.
(15) Farber, P.; Darmawan, H.; Sprules, T.; Mittermaier, A. *J. Am. Chem. Soc.* **2010**, *132*, 6214.
(16) Malgieri, G.; Russo, L.; Esposito, S.; Baglivo, I.; Zaccaro, L.; Pedone, E. M.; Di Blasio, B.; Isernia, C.; Pedone, P. V.; Fattorusso, R. *Proc. Natl. Acad. Sci. U.S.A.* **2007**, *104*, 17341.
(17) Baglivo, I.; Russo, L.; Esposito, S.; Malgieri, G.; Renda, M.; Salluzzo, A.; Di Blasio, B.; Isernia, C.; Fattorusso, R.; Pedone, P. V. *Proc. Natl. Acad. Sci. U.S.A.* **2009**, *106*, 6933.
(18) Zarrine-Afsar, A.; Larson, S. M.; Davidson, A. R. *Curr. Opin. Struct. Biol.* **2005**, *15*, 42.
(19) Naganathan, A. N.; Li, P.; Perez-Jimenez, R.; Sanchez-Ruiz, J. M.; Muñoz, V. *J. Am. Chem. Soc.* **2010**, *132*, 11183.
(20) Nickson, A. A.; Clarke, J. *Methods* **2010**, *52*, 38.
(21) Esposito, S.; Baglivo, I.; Malgieri, G.; Russo, L.; Zaccaro, L.; D'Andrea, L. D.; Mammucari, M.; Di Blasio, B.; Isernia, C.; Fattorusso, R.; Pedone, P. V. *Biochemistry* **2006**, *45*, 10394.
(22) Nomura, A.; Sugiura, Y. *Inorg. Chem.* **2002**, *41*, 3693.
(23) Isernia, C.; Bucci, E.; Leone, M.; Zaccaro, L.; Di Lello, P.; Digilio, G.; Esposito, S.; Saviano, M.; Di Blasio, B.; Pedone, C.; Pedone, P. V.; Fattorusso, R. *ChemBioChem* **2003**, *4*, 171.
(24) Chekmeneva, E.; Prohens, R.; Díaz-Cruz, J. M.; Ariño, C.; Esteban, M. *Anal. Biochem.* **2008**, *375*, 82.
(25) Blasie, C. A.; Berg, J. M. *Biochemistry* **2002**, *41*, 15068.
(26) Manetto, G. D.; Grasso, D. M.; Milardi, D.; Pappalardo, M.; Guzzi, R.; Sportelli, L.; Verbeet, M. P.; Canters, G. W.; La Rosa, C. *ChemBioChem* **2007**, *8*, 1941.
(27) La, R. C.; Milardi, D.; Grasso, D. M.; Verbeet, M. P.; Canters, G. W.; Sportelli, L.; Guzzi, R. *Eur. Biophys. J.* **2002**, *30*, 559.
(28) Milardi, D.; Arnesano, F.; Grasso, G.; Magrì, A.; Tabbì, G.; Scintilla, S.; Natile, G.; Rizzarelli, E. *Angew. Chem., Int. Ed.* **2007**, *46*, 7993.
(29) Hu, C. Q.; Sturtevant, J. M.; Thomson, J. A.; Erickson, R. E.; Pace, C. N. *Biochemistry* **1992**, *31*, 4876.
(30) Fischer, H.; Polikarpov, I.; Craievich, A. F. *Protein Sci.* **2004**, *13*, 2825.
(31) Foster, M. P.; Wuttke, D. S.; Clemens, K. R.; Jahnke, W.; Radhakrishnan, I.; Tennant, L.; Reymond, M.; Chung, J.; Wright, P. E. *J. Biomol. NMR* **1998**, *12*, 51.
(32) Mori, S.; Abeygunawardana, C.; Johnson, M. O.; van Zijl, P. C. *J. Magn. Reson., Ser. B* **1995**, *108*, 94.
(33) Bai, Y.; Milne, J. S.; Mayne, L.; Englander, S. W. *Proteins* **1993**, *17*, 75.
(34) Zhang, Y. Z.; Paterson, Y.; Roder, H. *Protein Sci.* **1995**, *4*, 804.
(35) Hvidt, A.; Nielsen, S. O. *Adv. Protein Chem.* **1966**, *21*, 287.
(36) Benson, E. E.; Linderstrom-Lang, K. *Biochim. Biophys. Acta* **1959**, *32*, 579.
(37) Berger, A.; Linderstrom-Lang, K. *Arch. Biochem. Biophys.* **1957**, *69*, 106.
(38) Linderstrom-Lang, K. *Biochim. Biophys. Acta* **1955**, *18*, 308.
(39) Bartels, C.; Xia, T. H.; Billeter, M.; Güntert, P.; Wüthrich, K. *J. Biomol. NMR* **1995**, *6*, 1.
(40) Koradi, R.; Billeter, M.; Wüthrich, K. *J. Mol. Graphics* **1996**, *14*, 51.
(41) Cohen, D. S.; Pielak, G. J. *Protein Sci.* **1994**, *3*, 1253.

(42) Malgieri, G.; Zaccaro, L.; Leone, M.; Bucci, E.; Esposito, S.; Baglivo, I.; Del Gatto, A.; Russo, L.; Scandurra, R.; Pedone, P. V.; Fattorusso, R.; Isernia, C. *Biopolymers* **2011**, *95*, 801.
(43) Blasie, C. A.; Berg, J. M. *Biochemistry* **2004**, *43*, 10600.
(44) Rich, A. M.; Bombarda, E.; Schenk, A. D.; Lee, P. E.; Cox, E. H.; Spuches, A. M.; Hudson, L. D.; Kieffer, B.; Wilcox, D. E. *J. Am. Chem. Soc.* **2012**, *134*, 10405.
(45) Russo, L.; Palmieri, M.; Baglivo, I.; Esposito, S.; Isernia, C.; Malgieri, G.; Pedone, P. V.; Fattorusso, R. *Biomol. NMR Assignments* **2010**, *4*, 55.
(46) Wishart, D. S.; Arndt, D.; Berjanskii, M.; Tang, P.; Zhou, J.; Lin, G. *Nucleic Acids Res.* **2008**, *36*, W496.
(47) Freire, E. *Methods Enzymol.* **1994**, *240*, 502.
(48) Muñoz, V.; Sanchez-Ruiz, J. M. *Proc. Natl. Acad. Sci. U.S.A.* **2004**, *101*, 17646.
(49) Mizuno, K.; Whittaker, M. M.; Bächinger, H. P.; Whittaker, J. W. *J. Biol. Chem.* **2004**, *279*, 27339.
(50) Huang, F.; Sato, S.; Sharpe, T. D.; Ying, L.; Fersht, A. R. *Proc. Natl. Acad. Sci. U.S.A.* **2007**, *104*, 123.
(51) Naganathan, A. N.; Sanchez-Ruiz, J. M.; Muñoz, V. *J. Am. Chem. Soc.* **2005**, *127*, 17970.
(52) Fung, A.; Li, P.; Godoy-Ruiz, R.; Sanchez-Ruiz, J. M.; Muñoz, V. *J. Am. Chem. Soc.* **2008**, *130*, 7489.
(53) Godoy-Ruiz, R.; Henry, E. R.; Kubelka, J.; Hofrichter, J.; Muñoz, V.; Sanchez-Ruiz, J. M.; Eaton, W. A. *J. Phys. Chem. B* **2008**, *112*, 5938.
(54) Bai, Y.; Sosnick, T. R.; Mayne, L.; Englander, S. W. *Science* **1995**, *269*, 192.
(55) Englander, S. W. *Annu. Rev. Biophys. Biomol. Struct.* **2000**, *29*, 213.
(56) Wilson, C. J.; Apiyo, D.; Wittung-Stafshede, P. *Q. Rev. Biophys.* **2004**, *37*, 285.
(57) Chang, S.; Jiao, X.; Hu, J. P.; Chen, Y.; Tian, X. H. *Int. J. Mol. Sci.* **2010**, *11*, 4014.
(58) Gopal, S. M.; Wenzel, W. *Angew. Chem., Int. Ed.* **2006**, *45*, 7726.
(59) Li, W.; Zhang, J.; Wang, J.; Wang, W. *J. Am. Chem. Soc.* **2008**, *130*, 892.
(60) Miura, T.; Satoh, T.; Takeuchi, H. *Biochim. Biophys. Acta* **1998**, *1384*, 171.
(61) Bai, Y. *J. Biomol. NMR* **1999**, *15*, 65.
(62) Bai, Y. *Chem. Rev.* **2006**, *106*, 1757.
(63) Yi, Q.; Baker, D. *Protein Sci.* **1996**, *5*, 1060.
(64) Muñoz, V.; Sadqi, M.; Naganathan, A. N.; de Sancho, D. *HFSP J.* **2008**, *2*, 342.
(65) Sborgi, L.; Verma, A.; Muñoz, V.; de Alba, E. *PLoS One* **2011**, *6*, e26409.
(66) Cho, S. S.; Weinkam, P.; Wolynes, P. G. *Proc. Natl. Acad. Sci. U.S.A.* **2008**, *105*, 118.